HHS Public Access

Author manuscript

Nat Struct Mol Biol. Author manuscript; available in PMC 2012 July 17.

Published in final edited form as:

Nat Struct Mol Biol. 2009 November ; 16(11): 1173–1177. doi:10.1038/nsmb.1713.

Molecular architecture of the Nup84–Nup145C–Sec13 edge element in the nuclear pore complex lattice

Stephen G. Brohawn and **Thomas U. Schwartz**

Department of Biology, Massachusetts Institute of Technology, 77 Massachusetts Avenue, Cambridge, MA 02139, USA.

Abstract

Nuclear pore complexes (NPCs) facilitate all nucleocytoplasmic transport. These massive protein assemblies are modular, with a stable structural scaffold supporting more dynamically attached components. The scaffold is made from multiple copies of the heptameric Y-complex and the heteromeric Nic96 complex. We demonstrated that members of these core subcomplexes specifically share an ACE1 fold with Sec31 of the COPII vesicle coat and proposed a lattice model for the NPC based on this commonality. Here we present the crystal structure of the heterotrimeric 134 kDa complex of Nup84-Nup145C-Sec13 of the Y-complex. The heterotypic ACE1 interaction of Nup84-Nup145C is analogous to the homotypic ACE1 interaction of Sec31 that forms COPII lattice edge elements and is inconsistent with the alternative “fence-like” NPC model. We construct a molecular model of the Y-complex and compare the architectural principles of COPII and NPC lattices.

In eukaryotic cells, physical separation of the nucleus and cytoplasm by the nuclear envelope (NE) necessitates a conduit for nucleocytoplasmic molecular traffic. This gateway is solely provided by nuclear pore complexes (NPCs), proteinaceous channels that stud the NE[1–4]. NPCs are among the largest assemblies in the cell at ~50 MDa and play critical roles in cellular homeostasis. The overall structure of the NPC has been shown to be generally conserved across species[5]. NPCs have a central scaffold ~30–50 nm in height with approximate eight-fold rotational symmetry about the transport axis, an outer diameter of ~100 nm, a central transport channel ~40 nm in diameter, and attached cytoplasmic and nucleoplasmic filaments[6–8]. The NPC is a modular structure composed of multiple copies of ~30 proteins (nucleoporins, Nups) arranged into distinct subcomplexes[4,9,10]. It is also dynamic, with components possessing widely ranging resident times[11,12]. The most stable Nups form the structural scaffold and are largely organized in the heteromeric Nic96

Correspondence should be addressed to T.U.S. (tus@mit.edu).

ACCESSION CODES

Protein Data Bank: The atomic coordinates for Nup145C$_{109–179}$•Sec13 and Nup84•Nup145C•Sec13 have been deposited with accession codes 3JRO and 3JRP, respectively.

AUTHOR CONTRIBUTIONS

S.G.B. designed, performed and analyzed biochemical, biophysical and crystallographic experiments and wrote the manuscript; T.U.S. advised on all aspects of the project and wrote the manuscript.

Methods and Supplementary Figures are available in the online version of the paper at http://www.nature.com/nsmb/.

subcomplex and the heptameric Y-complex. The scaffold connects to the NE through interaction with transmembrane Nups and anchors phenylalanine-glycine (FG) repeat-containing Nups that form an extended meshwork projecting into the central pore channel that constitutes the main transport barrier[13,14].

Considering its central role in transport and other cellular processes, a high-resolution structure of the NPC is much sought-after. Significant effort has focused on elucidating the central scaffold architecture. Its fundamental importance is evident as assembly defects coupled with transport deficiencies are observed by knockout/knockdown of scaffold components[15–20]. Still, the arrangement of the Nic96 subcomplex (including Nic96, Nup53/Nup59, Nup157/170, Nup188, Nup192; nomenclature from *S. cerevisiae* unless noted) remains largely enigmatic. However, the structures of major portions of Nic96, Nup170, and Nup53/59 are now available and combined with functional data will help narrow down the problem[21–24]. Organization of the Y-complex (composed of Nup133, Nup84, Nup145C, Sec13, Nup120, Nup85, and Seh1) is better understood. The complex is tightly associated and forms a Y observed by EM, with two short arms and a long kinked arm connected at a central hub[18,19,25–27]. High-affinity connections within the Y-complex involve binary interactions between α-helical domains of its constituents[26,28,29]. The long arm terminates with a flexibly attached N-terminal β-propeller of Nup133 followed by an irregular α-helical stack domain that interacts end-to-end with Nup84[29,30]. Nup84 in turn interacts with Nup145C. Nup120 and Nup85 form the short arms of the Y-complex, with the C-terminal region of Nup120 forming the central hub that interacts with the C-terminal tail modules of Nup145C and Nup85[31]. Nup145C and Nup85 bind the related β-propeller proteins Sec13 and Seh1, respectively, via addition of an N-terminal insertion blade to complete the open 6-bladed β-propellers *in trans*[28,32,33]. While crystallographic data on single proteins and some binary complexes are available, we are still lacking a detailed structural description of the entire Y-complex, notably including all domain-domain and protein-protein interfaces.

A common evolutionary origin of the NPC and vesicle coats had been proposed based on their shared role in stabilizing curved membranes and predicted similarities in fold composition of constituent proteins[34]. Structural evidence of a common ancestor was demonstrated as the nucleoporins Nic96, Nup85, Nup145C, and Nup84 are homologous to the COPII vesicle coatomer Sec31 and together constitute a unique fold class ACE1 (ancestral coatomer element 1)[28]. In the COPII vesicle coat lattice, two molecules of the ACE1 protein Sec31 interact to form edge elements, while the β-propellers of Sec31 and Sec13 interact to form vertex elements[35,36]. We proposed the NPC structural scaffold forms a similar lattice-like coat for the NE[28,37]. However, the absence of structural knowledge of ACE1 organization in the NPC precluded any direct comparison of the NPC and COPII lattices.

We set out to determine the molecular architecture of an edge element in the NPC lattice and here present the 4.0 Å crystal structure of the heterotrimeric Nup84•Nup145C•Sec13 unit of the Y-complex of the NPC from *S. cerevisiae*. The ACE1 interaction between Nup84 and Nup145C is architecturally related to the Sec31 edge element in the COPII lattice. As in the COPII coat, the edge element in the NPC lattice is arranged in a manner consistent with its role in stabilizing membrane curvature at the NE. We further present a composite atomic

model of the Y-complex, propose how it is arranged in the NPC, and compare the NPC lattice architecture to vesicle coats.

ONLINE METHODS

Construct generation

We cloned the trimeric complex of Nup84 (residues 1–424), Nup145C (109–555) and Sec13 from *S. cerevisiae* into a bicistronic bacterial expression vector. $Nup84_{1–424}$ was N-terminally fused with a cleavable 6xHis-tag. $Nup145C_{109–555}$ was C-terminally fused to Sec13 with a flexible 9-residue linker, to increase complex stability, without affecting chromatic behavior compared to the separate chain complex (data not shown)[28]. The trimeric complex is referred to as Nup84•Nup145C•Sec13 for simplicity. The completed β-propeller construct of Sec13 was generated by fusing the insertion blade of Nup145C (residues 109–179) C-terminally to full-length Sec13 via a flexible 9-residue linker. Sec13 was N-terminally fused with a cleavable 6xHis-tag.

Protein production and purification

Proteins were expressed in *E. coli* BL21-RIL(DE3) cells and purified as described[28]. Eluted protein was dialyzed against 50 mM Hepes-NaOH pH 7.4, 200 mM NaCl, 1 mM DTT, and 0.1 mM EDTA, the tag cleaved with protease overnight, and purified on a HiTrapS column (GE Healthcare) via a linear NaCl gradient followed by size exclusion chromatography. $Nup145C_{109–179}$•Sec13 was purified using a Superdex S75 26/60 column (GE Healthcare) run in 10 mM Tris-HCl pH 8.0, 150 mM NaCl, 1 mM DTT, and 0.1 mM EDTA. Nup84•Nup145C•Sec13 was purified using a Superdex S200 26/60 column (GE Healthcare) run in 10 mM Tris-HCl pH 8.0, 200 mM NaCl, 1 mM DTT, and 0.1 mM EDTA. Selenomethionine-derivatized Nup84•Nup145C•Sec13 was prepared as described[28] and purified as the native version with reducing agent concentration at 5 mM in all buffers.

Crystallization

Small crystals of $Nup145C_{109–179}$•Sec13 grew in hanging drops of 0.5 μl protein at 85 mg ml^{-1} and 0.5 μl precipitant (0.1 M Tris-HCl pH 8.3, 26.5% (w/v) PEG 4000, 0.25 M LiCl) at 16°C in three days and were processed for seeds. Diffraction quality crystals grew as large plates (300 × 300 × 10 μm) in hanging drops of 0.2 μl seed dilution, 0.5 μl protein at 38 mg ml^{-1}, and 0.5 μl precipitant (0.1M Tris-HCl pH 8.3, 22% (w/v) PEG 4000, 0.25 M LiCl) at 16°C in three days. Crystals were cryoprotected by briefly soaking in precipitant with 25% v/v glycerol and flash frozen in liquid nitrogen.

Diffraction quality crystals of Nup84•Nup145C•Sec13 grew as half-cylinders 25–50 μm in height with a radius of 50–200 μm in hanging drops of 0.25 μl protein at 22.5 mg ml^{-1} and 0.25 μl precipitant (1.15 M sodium malonate pH 5.7) at 22°C in 2 days. Selenomethionine derivatized protein crystallized under identical conditions. $[Ta_6Br_{12}]^{2+}$-derivatized crystals were obtained by transferring crystals into a 0.5 μl drop of 1.17 M sodium malonate pH 5.7 and 200 μM $[Ta_6Br_{12}]_{2+}$×$2Br^-$ (Jena Biosciences) and incubating for 1–2 hours. Crystals were cryoprotected by briefly soaking in precipitant with 22.5% v/v ethylene glycol and flash frozen in liquid nitrogen.

Data collection and structure determination

iMosflm[47] was used for data collection strategies, HKL2000[48] was used to reduce data, and model building and refinement were carried out with Coot[49] and Phenix[50].

A 20 μm aperture beam was used to collect data from separate spot regions of the $Nup145C_{109–179}$•Sec13 crystals because diffraction quality varied over their volume. Molecular replacement was accomplished with Phaser[51] using Sec13 (PDB ID 2PM6[35]) as a search model. The final model is missing the first two residues of Sec13, as well as loop residues 158–167. The final model has Ramachandran plot values of 95.4% favored, 4.3% allowed, and 0.3% outliers.

The structure of Nup84•Nup145C•Sec13 was solved with multiple isomorphous replacement with anomalous scattering (MIRAS) using selenomethionine and $[Ta_6Br_{12}]^{2+}$ derivatives. 12 selenium sites (out of 13) and 4 $[Ta_6Br_{12}]^{2+}$ sites were found with SHELXC/D/E[52] and refined in SHARP[53]. $Nup145C_{109–179}$•Sec13 (this work) and $Nup145C_{180–555}$ (PDB accession code 3BG1[32]) were placed into the solvent-flattened map from SHARP with BrutePTF[54]. PhaserEP[51] was used to refine selenium sites and the partial model. Discussion refers to the final selenomethionine crystal as it had a lower B factor and more interpretable maps than native crystals without any appreciable differences in the overall structure (data not shown). Residues 3–7 of Sec13, 554–555 of Nup145C, and 1–32 of Nup84 are not modeled, in addition to residues missing in $Nup145C_{109–179}$•Sec13. The absence of observed density for α1 of Nup84 may be due to the absence of ACE1 helix α17 in the crystal construct, which typically interacts with helix α1 in ACE1 proteins. The final model has Ramachandran plot values of 87.9% allowed, 10.9% allowed, and 1.2% outliers.

The high-resolution structure fragments superimpose well with the corresponding regions in the complete Nup84•Nup145C•Sec13 structure. $Nup145C_{109–179}$•Sec13 aligns with the same region in the trimeric structure with an average rmsd of 0.75 Å. The major difference is the orientation of the N-terminal 11 residues of Sec13. In the $Nup145C_{109–179}$•Sec13 structure, this region is extended away from the molecule and amino acids 3–8 from Sec13 form a strand E zipper closure with strand D from blade 2 of a neighboring Sec13 molecule. A short strand is formed from part of the loop connecting Sec13 and Nup145C and forms strand F. In the Nup84•Nup145C•Sec13 crystal, this interaction is not possible as there is not a symmetry related Sec13 molecule in an equivalent position. Instead, the N-terminus of Sec13 extends towards the N-terminal helix of Nup145C, though it is not modeled. We presume that the zipper interaction of two Sec13 molecules and the linker in the $Nup145C_{109–179}$•Sec13 structure is a crystal-packing artifact. Nup145C•Sec13 in the trimeric structure overlays well with the reported *S. cerevisiae* / *H. sapiens* hybrid structure with an average rmsd of 1.2 Å. The major difference between the two structures is a rotation of the Nup145C insertion blade/Sec13 unit of ~5–10° about the propeller axis. Whether this is a relevant movement of the molecules remains to be determined. Some rearrangement in the crown of Nup145C is observed in the current structure that is accounted for by reordering to form the interaction site for Nup84.

Structure analysis

Structure figures were made in Pymol (http://www.pymol.org). Interface calculations were performed using the PISA server[55]. Alignments were made with MUSCLE[56], analyzed in Jalview[57], and figures produced with Aline[58]. Structural superpositions were performed with Coot[59] and Cealign[60].

RESULTS

Structure of the Nup84•Nup145C•Sec13 trimeric complex

We solved the crystal structure of a trimeric complex between Nup84, Nup145C, and Sec13 from *S. cerevisiae* by MIRAS using selenomethionine and tantalum bromide derivatives (Fig. 1, Table 1). The crystallized construct includes $Nup84_{1–424}$, $Nup145C_{109–555}$, and full length Sec13. Despite modest resolution and relatively high B-factors, initial phase estimates were excellent and resulted in high-quality electron density maps (Supplementary Fig. 1). Still, confident model building at this resolution was aided by the availability of high-resolution models of fragments of the structure[38]. To this end, a complex of the minimal interaction domain of $Nup145C_{109–179}$ in complex with full-length Sec13 was crystallized, solved by molecular replacement at 2.6 Å resolution, and refined to an R_{work}/R_{free} of 21.5/25.3%. Placement of this partial model and $Nup145C_{180–555}$ from the *S. cerevisiae/H. sapiens* hybrid Nup145C•Sec13 structure[32] into the map was accomplished with real space methods. Phase improvement using the experimental data with the partial model resulted in clearly interpretable maps into which the final Nup84•Nup145C•Sec13 model was built and refined to an R_{work}/R_{free} of 28.2/32.9%.

The trimeric complex has the approximate shape of a kinked rod with dimensions ~ 150 × 30 × 30 Å (Fig. 1). Nup84 and Nup145C both form α-helical blocks with dimensions ~ 65×30×30 Å that interact at the kink in the rod creating a 2040 $Å^2$ interface. The N-terminus of Nup145C forms an insertion blade that completes the open 6-bladed β-propeller of Sec13 in trans. The higher resolution fragments both superimpose well with the same regions in the trimeric structure with mostly minor deviations observed (Supplementary Methods). In comparison to the hybrid human Sec13•yeast Nup145C structure[32], there is a ~10° rotation of the propeller unit about its central axis. This may be indicative of flexibility of the β-propeller unit relative to the ACE1 domain, which could be important in the assembly of the NPC lattice (see below)[36].

The ACE1 nucleoporins Nup84 and Nup145C interact crown·crown

As predicted by structural modeling, Nup84 adopts an ACE1 fold despite very low sequence homology to other ACE1 members (Supplementary Fig. 2)[28]. ACE1 is a tripartite, J-shaped helical fold composed of three modules: crown, trunk, and tail.

The Nup84•Nup145C•Sec13 structure contains the trunk and crown modules of Nup145C and Nup84 (Supplementary Fig. 2). The two proteins form an extensive interface between their crown modules with α6–α8 of Nup84 packing antiparallel to α6–α8 of Nup145C, completely burying α7 from each protein in the interface (Fig. 2a). The surfaces of helices α6-α8 in each protein are distinctly hydrophobic and highly conserved (Supplementary Fig.

3). Homodimerization of Sec31 is similarly accomplished by the antiparallel interaction of helices α6–8 (Fig. 2b)[35]. Interestingly, a domain swap between crown helices α5–α7 from each Sec31 monomer is observed in the crystal structure. Whether this is the physiologically relevant manner of interaction is unclear, but a long loop that allows for the domain swap is conserved in length in Sec31. Regardless, the interaction likewise juxtaposes and buries α7 from each Sec31 molecule.

Unique features of each ACE1 unit in the Nup84•Nup145C•Sec13 structure form additional interaction sites that frame the primary α6-α8 surface (Supplementary Fig. 3). Two extended and conserved loops in Nup84 (α3–α4 and α7–α8) pack against the long and kinked helix α4 of Nup145C. On the opposite side of the α6–α8 interface, Nup84 has an insertion of three short helices between ACE1 helices α4 and α5 (α4a–c) that together form an interface with the crown loops α6–α7 and α8–α9 of Nup145C.

Structural evidence for the lattice model of the NPC

By analogy to the Sec31 interaction in COPII coats, it was predicted that Nup84 and Nup145C would interact via their crown modules[28]. Surface point mutations in Nup145C α7 (V321E, S324E, Y325A) and corresponding mutations in the then predicted Nup84 helix α7 (I206D, M210D) were made, abrogating high-affinity binding. The structure presented here now definitively shows that the interaction between Nup84 and Nup145C is via ACE1 crown modules and allows the mutant data to be explained from a structural perspective. The mutated sites on each protein are intimately involved in the interaction surface: I206 and M210 account for 11% of the total area of Nup84 buried (223 of 2024 $Å^2$) while V321, S324, and Y325 form 12% of the total area of Nup145C buried (257 of 2059 $Å^2$). Introduction of charged residues into or loss of large side chains from the hydrophobic and complementary interaction surface is highly destabilizing, resulting in the specific disruption of the interaction. That these point mutations eliminate binding demonstrates that the α6–α8 surface is the primary binding determinant and the secondary framing interactions are insufficient to independently maintain interaction.

The Nup84•Nup145C•Sec13 structure presented here fully supports our lattice model for the NPC and provides conclusive evidence against the alternative “fence-like” model, based primarily on crystal contacts observed in the yeast Nup145C•human Sec13 hybrid structure[32]. In that crystal, Nup145C•Sec13 units stack via homotypic crown•crown interaction of Nup145C. Superposition of the Nup145C interaction observed in the crystal with the Nup84•Nup145C interface reported here shows that formation of the two interfaces is mutually exclusive (Supplementary Fig. 4).

Comparison of edge elements in the NPC and COPII coat

The similarity between the Nup84•Nup145C•Sec13 structure and the Sec13•Sec31 edge element in the COPII cage is immediately apparent (Fig. 3), thus we refer to the Nup84•Nup145C unit as an edge element in the NPC lattice. The shared binding mode between crown modules in the two structures results in analogous relative orientations of the interacting ACE1 units. The interface between Nup145C and Nup84 creates an angle of ~120° between ACE1 units. The interface between Sec31 molecules is ~165° in the crystal

structure, though it was modeled to be ~135° by normal mode analysis for fitting into both COPII coat EM reconstructions[35,36]. A hinge movement about the crown•crown interface was thus postulated to be one mechanism that allows the coat to adapt its size to vesicles of different diameter[35]. EM reconstruction of the Y-complex have similarly shown plasticity in the angles of the long arm[27]. Perhaps a similar hinge at the Nup84•Nup145C interface could be used in rearrangements of the NPC lattice in assembly and/or transport. Consistently, hinge movement at the crown·crown interface is observed in normal mode analysis of the Nup84•Nup145C•Sec13 structure (data not shown).

The insertion blade interaction between Sec13 and Nup145C or Sec31 is very similar in the two structures (data not shown). However, the different orientations of the insertion blade with respect to the ACE1 trunks result in Sec13 being positioned differently with respect to the edge elements. In the Sec31•Sec13 structure, the Sec13 propeller sits against the end of the Sec31 trunk, capping the edge element. In the Nup84•Nup145C•Sec13 structure, Sec13 is rotated ~45° forward towards the trunk and clockwise (viewed from the vertex) and rests on top of the Nup145C trunk. Whether additional interactions of Sec13 in the context of the entire NPC scaffold result in a conformational change from this position awaits to be seen.

DISCUSSION

The Nup84•Nup145C•Sec13 structure presented here together with the structures of Nup85•Seh1, Nup84•Nup133, and Nup120 previously reported[28,29,31,33] allows for the generation of a composite model for the majority of the Y-complex at high resolution, including relative orientations of components in the long arm (Fig. 4). The last four trunk helices of Nup84 need to be modeled to connect the Nup84•Nup145C•Sec13 and Nup84•Nup133 crystal structures. As these helices adopt identical topologies in other ACE1 structures and are predicted to be the only secondary structure elements present in Nup84 in this region, we can model their structure with high confidence (data not shown). This allows us to place the tail of Nup84 interacting with the full helical region of Nup133 relative to Nup84•Nup145C•Sec13. The position of the β-propeller of Nup133 is unknown and is probably flexible[30]. The tail modules of both Nup145C and Nup85 can be confidently modeled[28], however the C-terminal interaction domain of Nup120 cannot and is not shown. While the relative positions of the short arms with respect to the long arm of the Y-complex cannot be assigned unambiguously, we have chosen to model the β-propellers of Sec13 and Seh1 in close proximity to one another by analogy to the interactions of β-propellers at the vertex elements in the COPII coat[35,36]. While our positioning of the short arms is most consistent with all available data, we cannot currently exclude alternative arrangements.

Our model is generally consistent with the recently reported EM reconstruction of the Y-complex from yeast[27]. The angles of the Nup84•Nup145C and Nup84•Nup133 interfaces in our model correspond to those found in the highest frequency EM class-average. Here we incorporate ~ 0.5 MDa (of 0.58 MDa) of atomic models into a composite Y-complex model. Most importantly, the connecting Nup84•Nup145C•Sec13 structure allows for the incorporation of relative orientations of the proteins into the Y-complex model. Analysis of the Y-complex model reveals a number of functionally important implications.

Due to the high degree of conservation between edge element structures in the NPC and COPII lattices, we predict the same inner concave surface of the edge element will face the membrane in the NPC (Fig. 3B, 4). In this orientation, the N-terminal β-propeller/α-helical domain of Nup120 and the C-terminal α-helical domain of Nup133 point towards the membrane. These domains could potentially serve as attachment sites for additional nucleoporins that could connect the Y-complex to the membrane proximal and membrane-spanning Nups. Consistently, Nup120 has been shown to interact in vitro with Nup157, a member of the Nic96 subcomplex that can provide a link to transmembrane Nups[23,39]. The ACE1 containing Nup85 is positioned away from the membrane, where it may form interactions to propagate the NPC lattice. The N terminus of Nup145C is also oriented away from the membrane, allowing its binding partner Nup145N to project its FG-repeats into the pore channel[40].

The branch point in the Y-complex has the β-propeller proteins Sec13 and Seh1 available to generate potential vertex interactions in the NPC lattice similar to the Sec31 β-propellers vertex interactions in COPII coats. In contrast, at the opposite side of the NPC edge element Nup84 (unlike Nup145C, Nup85, and Sec31) does not interact with a β-propeller. Perhaps the loss of a β-propeller combined with the acquisition of the Nup133 “cap” have evolved as a way to terminate lattice propagation in this direction of the Y-complex long arm. The utility of this type of arrangement is unique to the cytoplasmic and nucleoplasmic facing sides of a NPC lattice, as it cannot form self-enclosed structures observed in vesicle coats.

Our model is consistent with a role for the NPC edge element in stabilizing membrane curvature. In other membrane coating systems, proteins that directly contact membranes display a positively charged surface for electrostatic interactions with membrane phospholipids[41–43]. Like clathrin and Sec31•Sec13, the NPC edge element is not found to display such a surface (Supplementary Fig. 5) and likely coats to stabilize, but not directly interact with, curved vesicle membranes. It should be noted that to date, the NPC has been shown only to be architecturally related to COPII coats while a relationship to clathrin coats[44] is limited to a shared fold composition of components[45]. Interestingly, an ALPS motif in human Nup133 has been shown to associate with membranes and has been suggested to initiate membrane curvature[46], though it has not been found in *S. cerevisiae*. This site is far enough removed from the ACE1 edge element that the Y- complex could play both roles; a curvature initiator at the distal end of the long arm and a lattice-integral stabilizer at the ACE1 edge element.

We favor a model in which the membrane facing edge element of the Y-complex is oriented parallel to the transport axis and serves to stabilize the positive membrane curvature of the NE, consistent with the evolutionarily relationship with the COPII edge element that stabilizes positive vesicle membrane curvature. While the resolution gap precludes a detailed comparison, our model is generally consistent with the recent computational model of the NPC[6]. As more high-resolution structures of components are solved, they may potentially be integrated to generate a more precise overall NPC structure. Fundamental to this goal will be the elucidation of potential vertex and inter-subcomplex interactions in the NPC lattice.

Supplementary Material

Refer to Web version on PubMed Central for supplementary material.

ACKNOWLEDGEMENTS

We thank staff at beamlines 24-ID-C/-E at Argonne National Laboratory for excellent assistance with data collection as well as the staff at beamline X29 at National Synchrotron Light Source for assistance in screening cryoprotection conditions through mail-in data collection service; Marko Gogala for his contributions to the Nup145C$_{109–179}$•Sec13 structure; Janet Iwasa for help with Figure 4; Members of the Schwartz laboratory for valuable discussions. This work was supported by an NIH grant (GM77537), a Pew Scholar Award (T.U.S.), and a Koch Fellowship Award (S.G.B).

References

1. Tran EJ, Wente SR. Dynamic nuclear pore complexes: life on the edge. Cell. 2006; 125:1041–1053. [PubMed: 16777596]
2. Weis K. Regulating access to the genome: nucleocytoplasmic transport throughout the cell cycle. Cell. 2003; 112:441–451. [PubMed: 12600309]
3. D'Angelo MA, Hetzer MW. Structure, dynamics and function of nuclear pore complexes. Trends Cell Biol. 2008; 18:456–466. [PubMed: 18786826]
4. Brohawn SG, Partridge JR, Whittle JRR, Schwartz TU. The nuclear pore omplex has entered the atomic age. Structure. 2009; 17:1156–1168. [PubMed: 19748337]
5. Elad N, Maimon T, Frenkiel-Krispin D, Lim RY, Medalia O. Structural analysis of the nuclear pore complex by integrated approaches. Curr Opin Struct Biol. 2009; 19:226–232. [PubMed: 19327984]
6. Alber F, et al. The molecular architecture of the nuclear pore complex. Nature. 2007; 450:695–701. [PubMed: 18046406]
7. Beck M, Lucic V, Forster F, Baumeister W, Medalia O. Snapshots of nuclear pore complexes in action captured by cryo-electron tomography. Nature. 2007; 449:611–615. [PubMed: 17851530]
8. Stoffler D, et al. Cryo-electron tomography provides novel insights into nuclear pore architecture: implications for nucleocytoplasmic transport. J Mol Biol. 2003; 328:119–130. [PubMed: 12684002]
9. Rout MP, et al. The yeast nuclear pore complex: composition, architecture, and transport mechanism. J Cell Biol. 2000; 148:635–651. [PubMed: 10684247]
10. Schwartz TU. Modularity within the architecture of the nuclear pore complex. Curr Opin Struct Biol. 2005; 15:221–226. [PubMed: 15837182]
11. Rabut G, Doye V, Ellenberg J. Mapping the dynamic organization of the nuclear pore complex inside single living cells. Nat Cell Biol. 2004; 6:1114–1121. [PubMed: 15502822]
12. Dultz E, et al. Systematic kinetic analysis of mitotic dis- and reassembly of the nuclear pore in living cells. J Cell Biol. 2008; 180:857–865. [PubMed: 18316408]
13. Rout MP, Aitchison JD, Magnasco MO, Chait BT. Virtual gating and nuclear transport: the hole picture. Trends Cell Biol. 2003; 13:622–628. [PubMed: 14624840]
14. Frey S, Gorlich D. A saturated FG-repeat hydrogel can reproduce the permeability properties of nuclear pore complexes. Cell. 2007; 130:512–523. [PubMed: 17693259]
15. Boehmer T, Enninga J, Dales S, Blobel G, Zhong H. Depletion of a single nucleoporin, Nup107, prevents the assembly of a subset of nucleoporins into the nuclear pore complex. Proc Natl Acad Sci U S A. 2003; 100:981–985. [PubMed: 12552102]
16. Fabre E, Hurt E. Yeast genetics to dissect the nuclear pore complex and nucleocytoplasmic trafficking. Annu Rev Genet. 1997; 31:277–313. [PubMed: 9442897]
17. Galy V, Mattaj IW, Askjaer P. Caenorhabditis elegans nucleoporins Nup93 and Nup205 determine the limit of nuclear pore complex size exclusion in vivo. Mol Biol Cell. 2003; 14:5104–5115. [PubMed: 12937276]
18. Harel A, et al. Removal of a single pore subcomplex results in vertebrate nuclei devoid of nuclear pores. Mol Cell. 2003; 11:853–864. [PubMed: 12718872]

19. Walther TC, et al. The conserved Nup107–160 complex is critical for nuclear pore complex assembly. Cell. 2003; 113:195–206. [PubMed: 12705868]
20. Makio T, et al. The nucleoporins Nup170p and Nup157p are essential for nuclear pore complex assembly. J Cell Biol. 2009; 185:459–473. [PubMed: 19414608]
21. Whittle JR, Schwartz TU. Architectural nucleoporins Nup157/170 and Nup133 are structurally related and descend from a second ancestral element. J Biol Chem. 2009
22. Jeudy S, Schwartz TU. Crystal structure of nucleoporin Nic96 reveals a novel, intricate helical domain architecture. J Biol Chem. 2007; 282:34904–34912. [PubMed: 17897938]
23. Onischenko E, Stanton LH, Madrid AS, Kieselbach T, Weis K. Role of the Ndc1 interaction network in yeast nuclear pore complex assembly and maintenance. J Cell Biol. 2009; 185:475–491. [PubMed: 19414609]
24. Schrader N, et al. Structural basis of the nic96 subcomplex organization in the nuclear pore channel. Mol Cell. 2008; 29:46–55. [PubMed: 18206968]
25. Siniossoglou S, et al. Structure and assembly of the Nup84p complex. J Cell Biol. 2000; 149:41–54. [PubMed: 10747086]
26. Lutzmann M, Kunze R, Buerer A, Aebi U, Hurt E. Modular self-assembly of a Y-shaped multiprotein complex from seven nucleoporins. Embo J. 2002; 21:387–397. [PubMed: 11823431]
27. Kampmann M, Blobel G. Three-dimensional structure and flexibility of a membrane-coating module of the nuclear pore complex. Nat Struct Mol Biol. 2009
28. Brohawn SG, Leksa NC, Spear ED, Rajashankar KR, Schwartz TU. Structural evidence for common ancestry of the nuclear pore complex and vesicle coats. Science. 2008; 322:1369–1373. [PubMed: 18974315]
29. Boehmer T, Jeudy S, Berke IC, Schwartz TU. Structural and Functional Studies of Nup107/Nup133 Interaction and Its Implications for the Architecture of the Nuclear Pore Complex. Mol Cell. 2008
30. Berke IC, Boehmer T, Blobel G, Schwartz TU. Structural and functional analysis of Nup133 domains reveals modular building blocks of the nuclear pore complex. J Cell Biol. 2004; 167:591–597. [PubMed: 15557116]
31. Leksa NC, Brohawn SG, Schwartz TU. The Structure of the Scaffold Nucleoporin Nup120 Reveals a New and Unexpected Domain Architecture. Structure. 2009
32. Hsia KC, Stavropoulos P, Blobel G, Hoelz A. Architecture of a coat for the nuclear pore membrane. Cell. 2007; 131:1313–1326. [PubMed: 18160040]
33. Debler EW, et al. A fence-like coat for the nuclear pore membrane. Mol Cell. 2008; 32:815–826. [PubMed: 19111661]
34. Devos D, et al. Components of coated vesicles and nuclear pore complexes share a common molecular architecture. PLoS Biol. 2004; 2:e380. [PubMed: 15523559]
35. Fath S, Mancias JD, Bi X, Goldberg J. Structure and Organization of Coat Proteins in the COPII Cage. Cell. 2007; 129:1325–1336. [PubMed: 17604721]
36. Stagg SM, et al. Structural basis for cargo regulation of COPII coat assembly. Cell. 2008; 134:474–484. [PubMed: 18692470]
37. Brohawn SG, Schwartz TU. A lattice model of the nuclear pore complex. Communicative and Integrative Biology. 2009; 2:1–3. [PubMed: 19704852]
38. Brunger AT, DeLaBarre B, Davies JM, Weis WI. X-ray structure determination at low resolution. Acta Crystallogr D Biol Crystallogr. 2009; 65:128–133. [PubMed: 19171967]
39. Lutzmann M, et al. Reconstitution of Nup157 and Nup145N into the Nup84 complex. J Biol Chem. 2005; 280:18442–18451. [PubMed: 15741174]
40. Ratner GA, Hodel AE, Powers MA. Molecular determinants of binding between Gly-Leu-Phe-Gly nucleoporins and the nuclear pore complex. J Biol Chem. 2007; 282:33968–33976. [PubMed: 17897945]
41. Zimmerberg J, Kozlov MM. How proteins produce cellular membrane curvature. Nat Rev Mol Cell Biol. 2006; 7:9–19. [PubMed: 16365634]
42. McMahon HT, Gallop JL. Membrane curvature and mechanisms of dynamic cell membrane remodelling. Nature. 2005; 438:590–596. [PubMed: 16319878]

43. Shibata Y, Hu J, Kozlov MM, Rapoport TA. Mechanisms Shaping the Membranes of Cellular Organelles. Annu. Rev. Cell Dev. Biol. 2009; 25:14.1–14.26.
44. Fotin A, et al. Molecular model for a complete clathrin lattice from electron cryomicroscopy. Nature. 2004; 432:573–579. [PubMed: 15502812]
45. Devos D, et al. Simple fold composition and modular architecture of the nuclear pore complex. Proc Natl Acad Sci U S A. 2006; 103:2172–2177. [PubMed: 16461911]
46. Drin G, et al. A general amphipathic alpha-helical motif for sensing membrane curvature. Nat Struct Mol Biol. 2007; 14:138–146. [PubMed: 17220896]
47. Leslie AGW. Recent changes to the MOSFLM package for processing film and image plate data. Joint CCP4 + ESF-EAMCB Newsletter on Protein Crystallography No. 26. 1992
48. Otwinowski Z, Minor W. Processing of X-ray diffraction data collected in oscillation mode. Methods in Enzymology. 1997; 276:307–326.
49. Emsley P, Cowtan K. Coot: model-building tools for molecular graphics. Acta Crystallogr D Biol Crystallogr. 2004; 60:2126–2132. [PubMed: 15572765]
50. Adams PD, et al. PHENIX: building new software for automated crystallographic structure determination. Acta Crystallogr D Biol Crystallogr. 2002; 58:1948–1954. [PubMed: 12393927]
51. McCoy AJ, et al. Phaser crystallographic software. J Appl Crystallogr. 2007; 40:658–674. [PubMed: 19461840]
52. Sheldrick GM. A short history of SHELX. Acta Crystallogr A. 2008; 64:112–122. [PubMed: 18156677]
53. Vonrhein C, Blanc E, Roversi P, Bricogne G. Automated structure solution with autoSHARP. Methods Mol Biol. 2007; 364:215–230. [PubMed: 17172768]
54. Strokopytov BV, et al. Phased translation function revisited: structure solution of the cofilin-homology domain from yeast actin-binding protein 1 using six-dimensional searches. Acta Crystallogr D Biol Crystallogr. 2005; 61:285–293. [PubMed: 15735338]
55. Krissinel E, Henrick K. Inference of macromolecular assemblies from crystalline state. J Mol Biol. 2007; 372:774–797. [PubMed: 17681537]
56. Edgar RC. MUSCLE: multiple sequence alignment with high accuracy and high throughput. Nucleic Acids Res. 2004; 32:1792–1797. [PubMed: 15034147]
57. Waterhouse AM, Procter JB, Martin DM, Clamp M, Barton GJ. Jalview Version 2--a multiple sequence alignment editor and analysis workbench. Bioinformatics. 2009; 25:1189–1191. [PubMed: 19151095]
58. Bond CS, Schuttelkopf AW. ALINE: a WYSIWYG protein-sequence alignment editor for publication-quality alignments. Acta Crystallogr D Biol Crystallogr. 2009; 65:510–512. [PubMed: 19390156]
59. Krissinel E, Henrick K. Secondary-structure matching (SSM), a new tool for fast protein structure alignment in three dimensions. Acta Crystallogr D Biol Crystallogr. 2004; 60:2256–2268. [PubMed: 15572779]
60. Jia Y, Dewey TG, Shindyalov IN, Bourne PE. A new scoring function and associated statistical significance for structure alignment by CE. J Comput Biol. 2004; 11:787–799. [PubMed: 15700402]

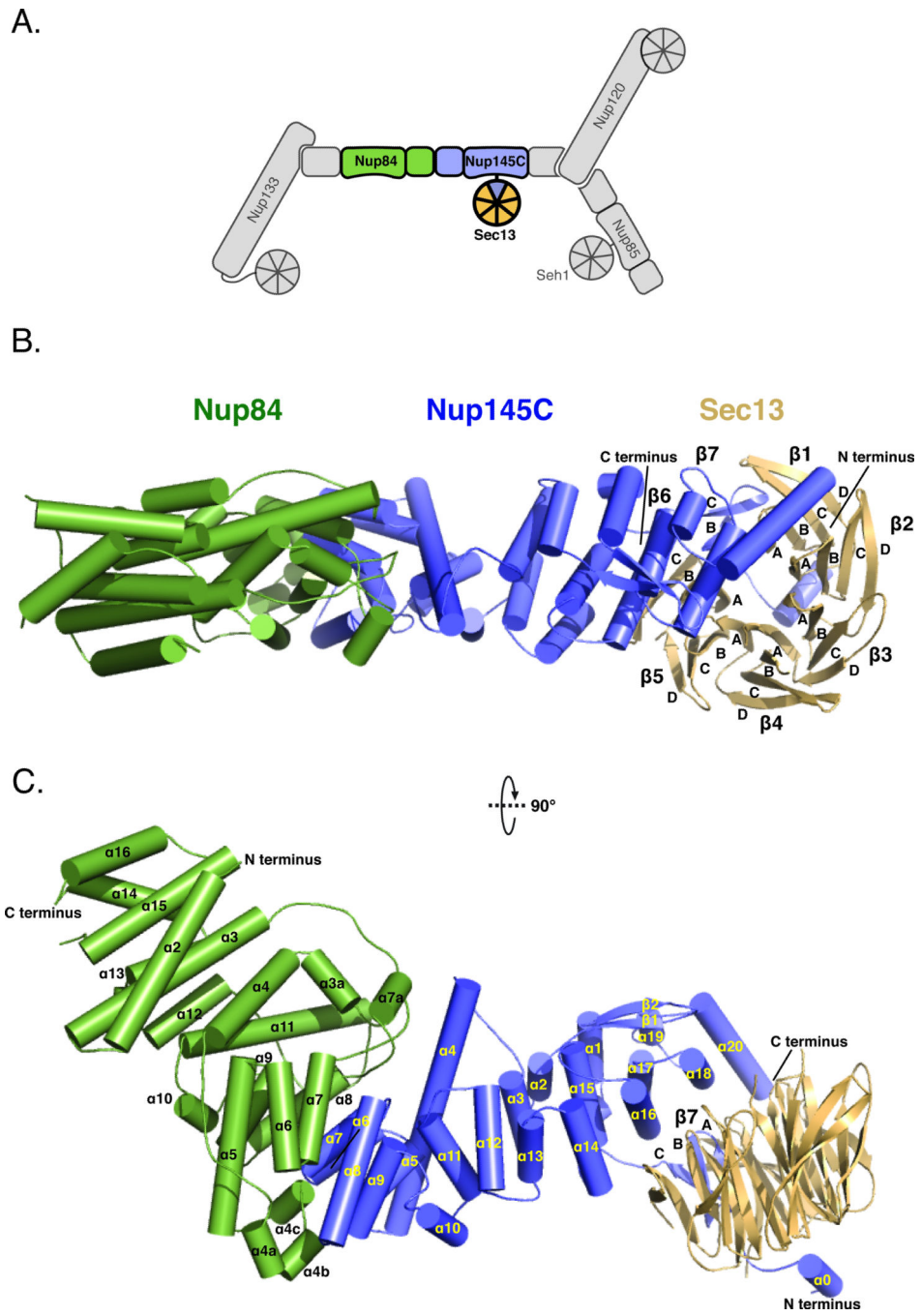

Figure 1. Structure of Nup84•Nup145C•Sec13

(A) Schematic diagram of the Y-complex of the nuclear pore complex (NPC). The crystallized trimeric segment is colored. (B-D) The overall structure of the heterotrimeric Nup84•Nup145C•Sec13 complex is shown with Nup84 in green, Nup145C in blue, and Sec13 in light orange. (B) The β-propeller composed of blades 1–6 from Sec13 and blade 7 from Nup145C is labeled. (C) Structure rotated by 90°, with secondary structure elements of Nup84 and Nup145C labeled.

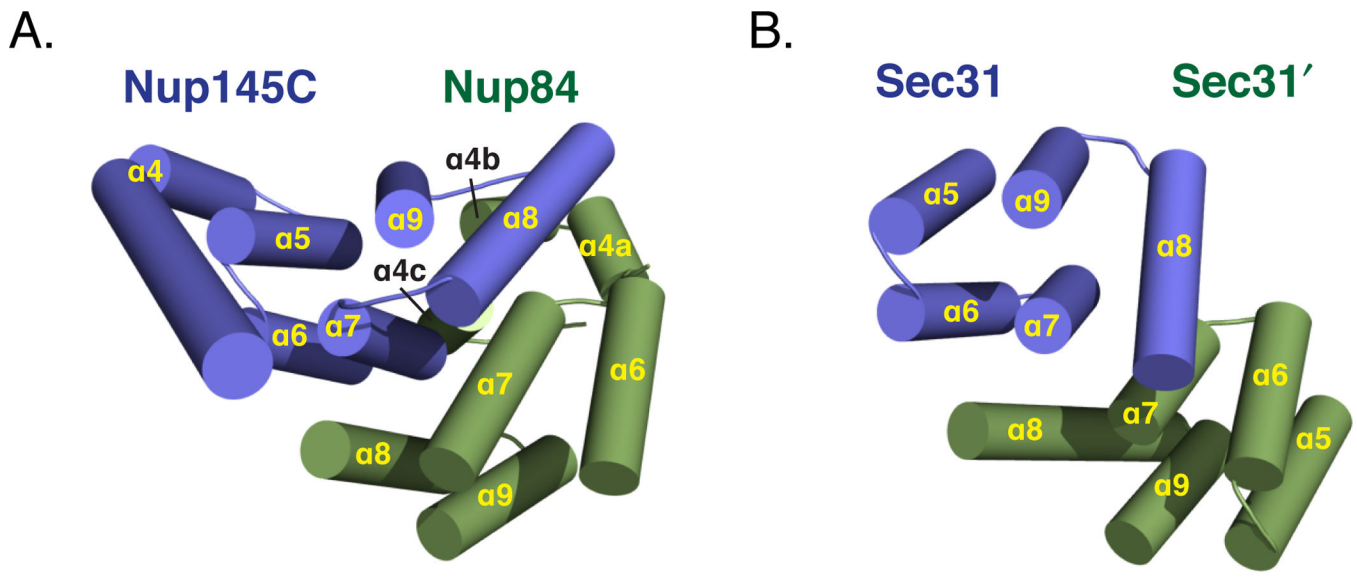

Figure 2. The crown•crown interaction of Nup84•Nup145C is analogous to Sec31•Sec31

The ancestral coatomer element 1 (ACE1) crown•crown interaction between Nup145C and Nup84 is shown in (A) and between two molecules of Sec31 in (B). In (B), The Sec31 interaction is shown non-domain swapped and the remainders of the molecules are removed for clarity (see main text). Analogous juxtaposition of crown helices α6–α8 is observed in both structures.

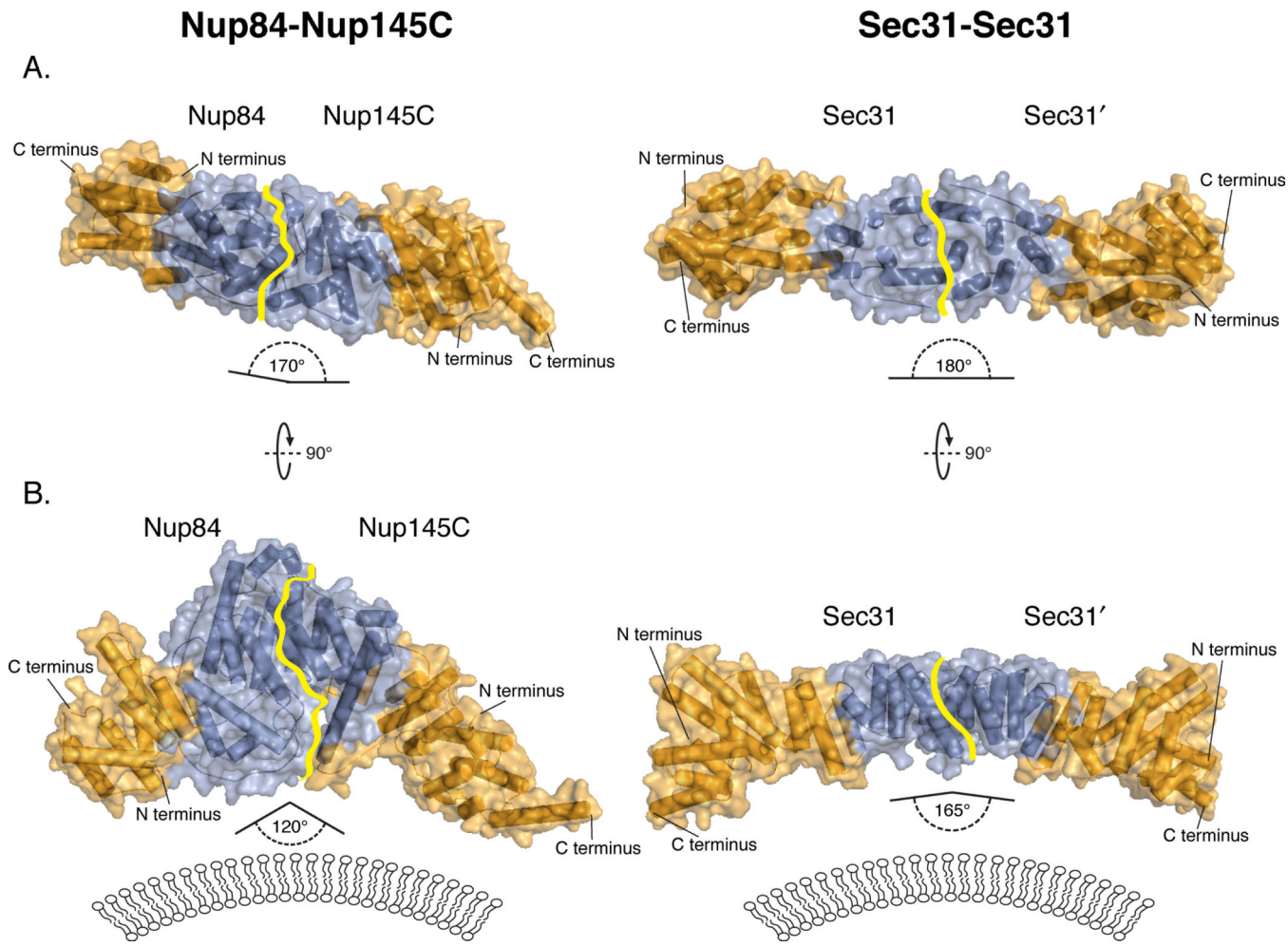

Figure 3. Comparison of edge elements in the NPC and COPII lattices

The lattice edge element Nup84•Nup145C in the NPC and Sec31•Sec31 (PDB: 2PM6[35]) in the COPII vesicle coat are shown as cartoons in a half-transparent surface. The two ACE1 units in each edge element are colored by module, with trunks orange and crowns blue. A yellow line indicates the interface between crown modules. The structures are shown from a top view in (A) (180° rotated from Figure 1A) and a side view rotated by 90° in (B). The analogous crown•crown interactions result in edge elements that share a common architectural arrangement. Viewed from the top, the Nup84•Nup145C edge element is bent ~10° from horizontal, while the Sec31•Sec31 edge is essentially straight. Viewed from the side, the crystal structures of the edge elements show dramatically different angles with the Nup84•Nup145C edge 45° more acute than Sec31•Sec31. The angle observed in the Nup84•Nup145C edge corresponds closely to the angle the Sec31•Sec31 interface was modeled to for fitting into the EM reconstructions of the COPII cage and coat [35,36]. The proposed position of the nuclear envelope (NE) membrane relative to the NPC edge element shown in (B) is analogous to the known position of the COPII vesicle membrane relative to the COPII edge element.

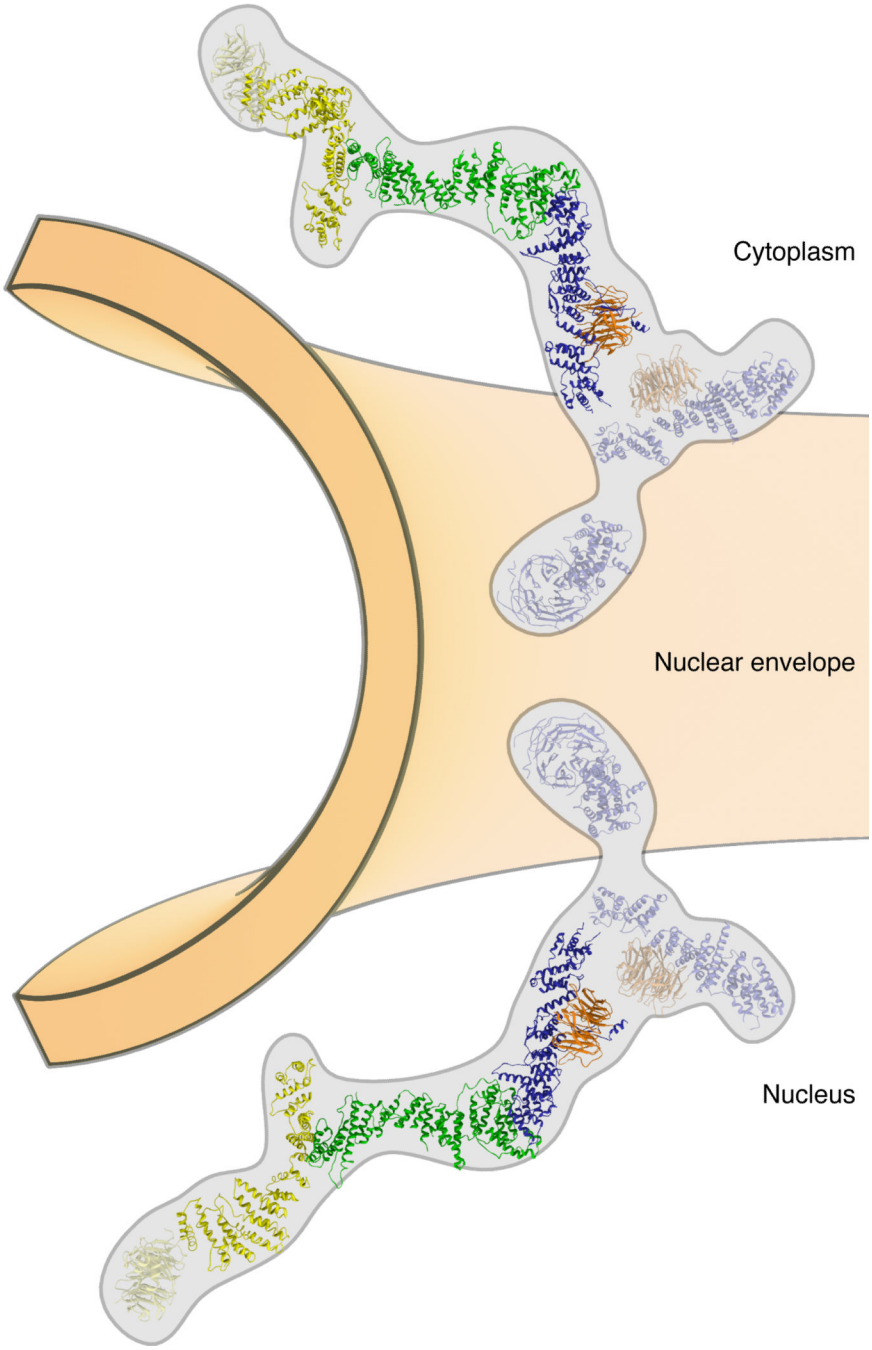

Figure 4. Nup84•Nup145C is a membrane curvature-stabilizing edge element in the NPC lattice

A composite atomic model for the Y-complex of the NPC emphasizing the role of the Nup84•Nup145C edge element as a membrane curvature-stabilizing unit, analogous to the Sec31•Sec31 edge element in COPII vesicle coats. The long arm of the Y-complex is a composite model from crystal structures and is shown with Nup145C blue, Sec13 orange, Nup84 green, and Nup133 yellow. The relative position of the N-terminal propeller of Nup133 (yellow) and the short arm components Nup120 (blue) and Nup85 (blue)•Seh1 (orange) are more tentatively placed and shown half-transparent (see text for details). The

long axis of the Y-complex is oriented along the positively curved NE membrane with the concave face of the Nup84•Nup145C edge element facing the lipid bilayer. This orientation is analogous to that of the Sec31•Sec31 edge element in the COPII coat and is consistent with the evolutionary relationship between the NPC and COPII vesicle coat lattices. Importantly, while the Y-complex is shown facing the membrane, it is not predicted to directly contact the NE. Rather, other Nups are predicted to play roles that correspond to adaptor complexes in other vesicle coating systems that link the membrane curvature-stabilizing coat (the Y-complex) to the NE.

Data collection and refinement statistics

	Nup145C$_{109–179}$- Sec13 Native	Nup84•Nup145C•Sec13 Selenomethionine	Nup84•Nup145C•Sec13 $[Ta_6Br_{12}]^{2+}$
Data collection			
Space group	$P2_12_12$	$P6_222$	$P6_222$
Cell dimensions			
a, *b*, *c* (Å)	68.3, 93.9, 55.0	170, 170, 271	170, 170, 270
α, *β*, *γ* (°)	90, 90, 90	90, 90, 120	90, 90, 120
Resolution (Å)	40-2.6 (2.66-2.6) *	50-4.0 (4.14-4.0)	50-4.4 (4.56-4.4)
R_{sym} (%)	12.6 (64.9)	17.2 (97.4)	17.0 (79.9)
$I/\sigma I$	12.4 (2.0)	10.6 (1.5)	8.6 (1.3)
Completeness (%)	97.9 (96.9)	99.9 (99.9)	92.2 (76.6)
Redundancy	3.5 (3.3)	5.9 (5.0)	3.7 (2.2)
Refinement			
Resolution (Å)	35-2.6	50-4.0	
No. reflections	11148	37016	
R_{work} / R_{free}	21.7 / 25.4	28.2 / 32.9	
No. atoms			
Protein	2621	8671	
Water	67	0	
B-factors (Å^2)			
Protein	71	189	
Water	70	n/a	
R.m.s deviations			
Bond lengths (Å)	0.003	0.004	
Bond angles (°)	0.679	0.762	

* Values in parentheses are for highest-resolution shell.